

# APPLICATION OF MOLECULAR DYNAMICS FOR LOW ENERGY ION IMPLANTATION IN CRYSTALLINE SILICON

H. Y. Chan and M. P. Srinivasan

Department of Chemical and Biomolecular Engineering, National University of Singapore,  
9 Engineering Drive 1, Singapore 117576

N. J. Montgomery, C. P. A. Mulcahy and S. Biswas

Cascade Scientific Ltd, ETC Building, Brunel Science Park, Uxbridge UB8 3PH, U.K.

H. -J. L. Gossmann and M. Harris

Axcelis Technologies, 108 Cherry Hill Drive, Beverly, MA 01915-1053, USA

K. Nordlund

Accelerator Laboratory, P.O. Box 43, FIN-00014 University of Helsinki, Finland

F. Benistant, C. M. Ng, D. Gui and L. Chan

Chartered Semiconductor Manufacturing Ltd., 60 Woodlands Industrial Park D, Street 2,  
Singapore 738406

Molecular Dynamics (MD) is set to replace Monte Carlo (MC) methods utilizing the Binary Collision Approximation (BCA) in modeling dopant distributions after ion implantation in the low energy regime. Simultaneous non-binary interactions come into play as the ion slows down; Unlike BCA, MD automatically accounts for multiple collisions between ion and its neighboring atoms. In this work, the energy limit below which BCA fails is estimated from density functional theory (DFT) calculations for a wide range of dopants. Impurity profiles are generated using the MD code, MDRANGE. A database consisting of Secondary Ion Mass Spectrometry (SIMS) profiles covering a wide range of dopants (B, C, F, N, P, As, Ge, In and Sb) over the energy regime of 0.5-10keV at critical channeling directions have been set up. The MD simulated profiles show good agreement with SIMS data, which have been obtained either with a quadrupole- or magnetic-sector- based mass spectrometer.

## 1. INTRODUCTION

In modeling ion implantation, the impact process of ions in solids is often treated by binary sequences of the projectile atom and one target atom in a solid. The "binary collision" approximation (BCA) (1) is supported by the fact that the range of significant interatomic force for the collision is shorter than distances of target atoms in the bulk because of the screening effect and that the collision process lasts for time periods in the order of  $10^{-15}$  seconds, which is significantly shorter than the lattice vibration period of atoms. Under the binary collision approximation, the implant range and distribution of implanted atoms in a solid can be determined by analytical solution of the stochastic process (2). However, as the demand continues for improving key technological parameters in silicon-based ion implantation technology, smaller device feature sizes are required down to the nanometer regime, which equates to ultra-shallow highly doped junctions in devices structures. Lower implantation energies are required and the dopant profiles should be controlled to tolerances of a few tenths of nm. The basic assumption of BCA stating the potential energy of the ion at the start of the collision to be negligible as compared to its kinetic energy should be questioned and its use re-examined at very low implantation energies. Another deficiency of BCA is that it neglects multi-body interactions, which become important when the interatomic potentials of not only the nearest target, but of more distant ones, become non-negligible. This can happen at low ion energies, as well as in crystal channels at higher energies.

In order to accurately analyze the collision process between ion and target at low energies, it is desirable to describe the motion of all the atoms involved in the process, and this can be done by numerically solving Newton's equations of motion for all atoms in the system, a technique known as Molecular Dynamics (MD). While MD simulations are limited in time and space as compared to BCA, the advent of supercomputers and the fact that the collision cascades formed at low energies are small makes MD a feasible and popular solution these days. Moreover, the number of free parameters is limited and its accuracy in many-body collisions in the low energy regime warrants its use. In this work, all simulated range profiles have been generated using the MD code, MDRANGE (3) with the recoil interaction approximation (RIA). A brief description of the models used in this code can be found in the ensuing sections. The interatomic potentials between ion and target have been calculated using density functional theory (DFT) methods for each specific ion-target pair, and the energy at which BCA reaches the brink of its applicability have been estimated from the potential energy curves for a wide range of industrially important dopants. A comprehensive database consisting of 70 low-energy Secondary Ion Mass Spectrometry (SIMS) profiles of nine dopants (B, C, N, F, P, Ge, As, In and Sb) over the energy range 0.5-10keV at doses  $5e13$ - $1e15$  atoms/cm<sup>2</sup> and implant tilts of 7°, 0° and 45° has been set up for the calibration of low energy implant profiles. Good agreement between experimental and simulation results has been obtained, especially for the 45° channeling implants and will be shown in the final section. This work shows the use of MD not only for typical non-channeling implants, but its accuracy in describing long-ranged profiles propagated in crystal channels makes MD a robust technique in modeling dopant profiles at both low and high implantation energies.

## 2. ESTIMATION OF BCA BREAKDOWN ENERGIES

The validity of BCA and the useful range of application of molecular dynamics simulations with the Recoil Ion Approximation (MD-RIA) have been addressed by Hobler et al (4). In his work, the validity of MD-RIA down to energies well below 100eV has been ascertained. BCA, however, has a more restricted range of applicability than MD-RIA. The upper limit,  $E_{min}^{BCA}$  at which BCA breaks down has been estimated as a function of the projectile's mass,  $M_x$ , in amu (4), as shown in Eq. 1.

$$E_{min}^{BCA} = 30M_x^{0.55} \text{ eV} \quad \text{Eq. 1}$$

The actual breakdown limit has never been clearly defined because BCA fails gradually as the energy lowers. Thus the limits also depend on the accuracy level used.  $E_{min}^{BCA}$  has been calculated for eleven industrially common dopants based on Eq. 1 and the values are given in the second column of Table I.

Element (X)	Ref (4)	UT-Tables	BCA code (6)	DFT(NN <sub>Si</sub> )
B	0.111	0.5	0.5	0.429
C	0.118	-	-	0.515
N	0.128	-	-	0.601
F	0.152	0.5	2	0.772
Si	0.188	-	1	1.202
P	0.198	15	5	1.287
Ga	0.310	-	-	2.661
Ge	0.317	-	10	2.746
As	0.322	0.5	1	2.832
In	0.407	-	5	4.205
Sb	0.421	-	-	4.377

Table I Estimated energy limits below which BCA breaks down. All values shown are in units of keV.

Column 3 of Table I shows the lower energy limit for some elements taken from the University of Texas Range Parameter tables (also known as Al Tasch tables) (5). The 4<sup>th</sup> column reflects this limit for the Monte Carlo BCA code UT-MARLOWE (6). Clearly, the low values calculated from Eq. 1 seem to suggest that BCA is valid down to the sub-keV range, even for heavy species like In and Sb, while the justifiable range of use for common BCA codes is restricted to much higher energies for heavier elements.

The last column reflects estimations of the breakdown limit based on DFT calculations for each projectile-target pair. These values are obtained based on the assumption that BCA fails when the kinetic energy of the ion becomes comparable to the unscreened nucleus-nucleus Coulombic repulsion of the ion and target atom, at a distance corresponding to the nearest neighbor separation. For silicon, this distance corresponds to 2.351Å, which is given by Eq. 2 with “a” being the lattice cell parameter, 5.431Å.

$$R_{\text{NNSI}} = \frac{\sqrt{3}a}{4} = \frac{\sqrt{3} \times 5.431}{4} = 2.351 \text{ \AA} \quad \text{Eq. 2}$$

The interatomic potential energies for each projectile-target pair have been calculated with the DMOL package (7) which utilizes numerical basis sets and are shown in Fig 1. Details of the DFT calculations can be found in (8). Hydrogenic orbitals were included for all systems studied. Although the breakdown limits for the different species have been calculated with diatoms, which are simple approximations to the true multi-body interacting forces in the repulsive, repulsive-attractive transition and attractive regions, it has been suggested that the diatomic potential does not differ much from a bulk potential at energies  $\geq 10\text{eV}$  (8). The limiting kinetic energies shown in the last column are taken to be the *absolute* coulomb nuclear repulsion energies at interatomic distances corresponding to  $R_{\text{NNSI}}$ . The calculated limits are significantly higher compared to the limits given by Eq. 1 while they show more coherence with those given by the BCA code for B, Si and In.

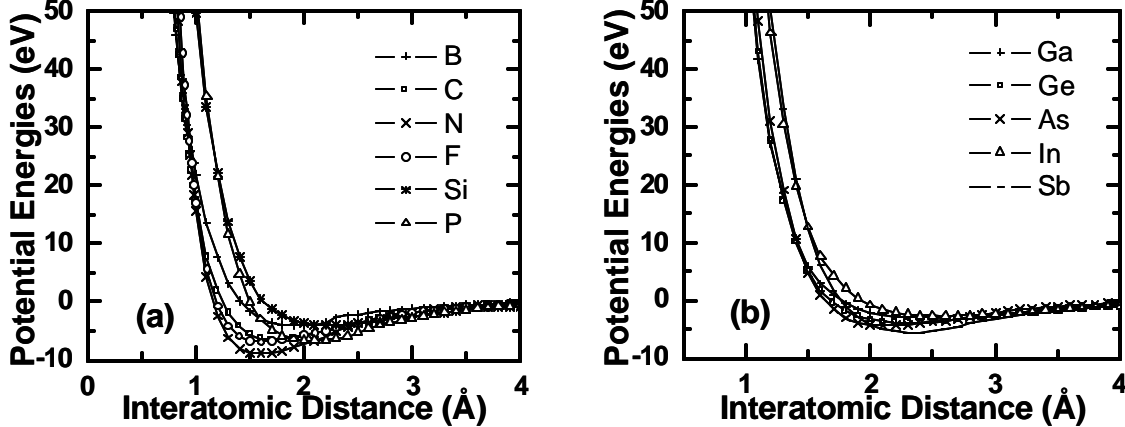


Fig. 1 Pair potential energy curves calculated for different species with silicon as the target atom.

Similar to the function suggested by Hobler et al in (4), the breakdown limit estimated from the DFT-calculated pair potentials in this work suggests a power-law relationship with the atomic mass,  $M_x$  and a linear relationship with atomic number,  $Z_x$  (Fig. 2). The dependence of the breakdown limit on the mass of the projectile can be attributed to the larger interaction distance for larger ions. Suppose the projectile approaches with an initial kinetic energy of 100eV, the incoming ion can achieve a maximum interaction potential of 50eV in a head-on collision based on a center-of-mass coordinate system. Based on the potentials calculated for X-Si in Fig. 1, the distance of closest approach between light elements like B, C, N and F and the target atom Si is circa 0.8Å. For heavy elements like In and Sb, this screening envelope extends to approximately 1.2Å. This larger screening effect of the heavy ions negates the importance of many-body nuclear effects as compared to the smaller ions, which experiences a higher probability of simultaneous collisions with the neighboring target atoms as energy lowers. The light ions' susceptibility to the multi-body interactions defeats the binary collision approximation and explains their lower breakdown limit compared to the heavy ions, which are more effectively shielded against the surrounding atoms.

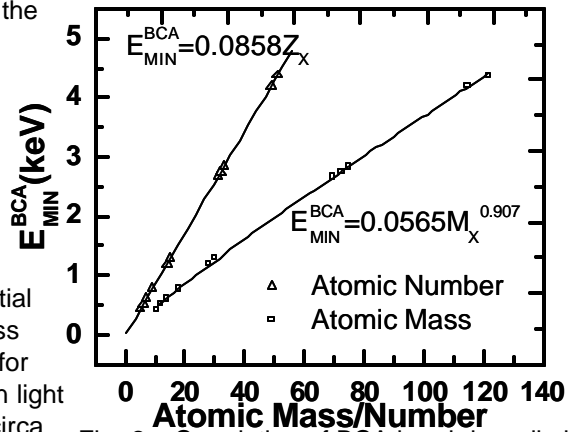


Fig. 2 Correlation of BCA breakdown limits calculated by DFT with atomic mass (power law) and atomic number (linear)

### 3. MOLECULAR DYNAMICS SIMULATIONS

The simulated profiles shown in this work have been obtained from the MD code, MDRANGE (3). The nuclear stopping has been treated with the DFT calculated potentials shown in Fig. 1. The Recoil Ion Approximation (RIA) has been employed, where only the ion-recoil interactions are considered. This is based on the assumption that the interactions between the ion and its nearest neighbors are much stronger than the lattice-lattice interactions. RIA has been shown to reduce the computational burden, with little effect on the final range profiles (3).

The electronic stopping model used affects the distribution of low energy doping ions, especially in high channeling directions. The channeling of ions during the slowing down process has an important impact on the concentration profiles both in the vertical and lateral directions. In crystal channels, where the atomic and electronic densities are significantly lower than average, the importance of nuclear stopping is reduced relative to the electronic stopping in crystal channels and it is imperative that the electronic stopping model predict the ranges of the channeled ions accurately. A local electronic stopping model is adopted since a non-local model is not likely to work where the electron density in a channel is significantly lower than in other directions. This model is based on scattering phase shifts for Fermi-surface electrons (9). The electronic stopping power of the ion,  $S_E$  traveling at velocity  $v$ , in a homogeneous electron gas can be expressed as in Eq. 3, where  $k_F$  is the Fermi momentum of electrons of the target,  $r_s$  is the one-electron radius (function of the electron density) and  $\delta_l(E_F)$  is the phase shift at quantum number  $l$  for the scattering of an electron at the Fermi energy  $E_F$ .

$$S_E = \frac{3v}{k_F r_s^3} \sum_{l=0}^{\infty} (l+1) \sin^2[\delta_l(E_F) - \delta_{l+1}(E_F)] \quad \text{Eq. 3}$$

The scattering phase shifts  $\delta_l(E_F)$  can be determined within the density functional theory for atoms embedded in a homogeneous electron gas (10) and are calculated in this work for  $Z=5$  through  $Z=51$  (all eleven elements shown in Table I). A dense grid of one-electron radius  $r_s$  values  $0.1\text{\AA} \leq r_s \leq 6\text{\AA}$  is employed and components up to  $l=10$  were used, although phase shifts for  $l > 5$  are very small. In cases where a self-consistent solution could not be obtained, which occurs for In and Sb, the Fermi phase shifts are calculated for a reduced grid of  $r_s$  values, and the tabulated values are then used in interpolating the phase shifts for a desired electron density. The anisotropy of the electron distribution is taken into account by using a three-dimensional charge distribution of silicon (11).

In all the simulations, initially crystalline silicon was used as a target material. A native amorphous oxide layer on the surface was taken into account and measured experimentally to be  $10 \pm 1\text{\AA}$  in all cases. The surface temperature of the experiments, 300K was used and realistic atomic thermal displacements were obtained by setting the Debye temperature of silicon to 519K (11). The number of simulated ions used was 20,000, and deemed sufficient for good statistics. In order to determine the profiles over more than four decades of concentration, a version of Beardmore's rare-event algorithm (12) was implemented. An atom splitting scheme is employed so that at certain splitting depths the ion is split into two virtual ions with a statistical weight of half that of the unsplit ion (13). This ensures accurate dopant profiles with good statistics and feasible computational overhead. The effect of damage build-up on range profiles is especially pronounced at low energies and is taken into account by changing the material structure in front of the path of the incoming ion (14).

### 4. LOW ENERGY SIMS DATABASE

The experimental data in this work has been obtained either by quadrupole- or magnetic-sector-based Secondary Ion Mass Spectrometry (SIMS). It is imperative to validate range profiles in the low energy regime as integrated-circuit device size shrinks, not only for common source-drain dopants like B and As, but also for heavy elements like In and Sb which play a crucial role in minimizing punch-through, channel engineering and threshold voltage adjustment.

A comprehensive SIMS database was set up to calibrate low energy profiles for nine industrially important dopants, namely B, C, N, F, P, Ge, As, In and Sb. The energy range for each dopant was chosen such that the energies span across the BCA breakdown limits as shown in the last column of Table I. The dose ranges from  $5e13$ - $1e15$  atoms/cm<sup>2</sup> and the implant tilt/twist angles investigated are 7°/22°, 0°/0° and 45°/45°, which corresponds to increasing levels of channeling respectively. The tilt angle is the angle between the incident ion beam and the normal of the wafer plane, while the azimuthal angle is measured with respect to the (100) plane in which the implants take place. While tilting the wafer surface relative to the incident ion beam direction by 7° is a widely adopted procedure to minimize channeling, the use of self-aligned (0° tilt) source-drain extension doping is inevitable. Although tilt angles of 45° are not yet common in wafer fabrication process, a wafer orientation of 45° in the azimuthal direction, in addition to the 45° tilt angle, represents one of the worst scenarios in axial and planar channeling (15). Such profiles should be well calibrated for profiles implanted in any direction to be modeled accurately. Table II summarizes the implant conditions used in setting up the database.

Element (X)	Energy (keV)	Dose (atoms/cm <sup>2</sup> )	Tilt/Twist (°)
B	0.5	5e13 – 1e14	45°/0° - 54°
C	0.5 - 2	1e14	0°/0° and 45°/45°
N	0.5 - 10	1 <sup>e</sup> 14, 1 <sup>e</sup> 15	7°/22°, 0°/0° and 45°/45°
F	1 - 5	6e13	0°/0° and 45°/45°
P	1 - 5	5 <sup>e</sup> 13 – 1e15	7°/22°, 0°/0° and 45°/45°
Ge	2 - 5	5e13	0°/0° and 45°/45°
As	2 - 10	5 <sup>e</sup> 13 – 1e15	7°/22°, 0°/0° and 45°/45°
In	2 - 10	5e13	0°/0° and 45°/45°
Sb	2 - 10	5e13 – 1e14	7°/22°, 0°/0° and 45°/45°

Table II Implant conditions for 70-wafer split involving nine species.

For quadrupole SIMS analysis, a Phi Adept 1010 quadrupole SIMS instrument has been used; a 750eV, 100nA Cs+ beam looking at negative secondary ions at 60° incidence angle with the sample potential held at zero voltage. The magnetic-sector SIMS have been obtained with a Cameca IMF Wf instrument with a 60° float column. A 10nA Cs+ beam with net impact energy of 520eV was used to bombard the sample biased at -3kV at grazing 70° incidence angle. There is no voltage offset on the samples

## 5. COMPARISONS WITH EXPERIMENTAL DATA

Figs. 3 to 8 show the comparisons between some of the representative experimental SIMS data and simulated profiles from MDRANGE and a BCA-based code for various species. Figs 3a to 8a show the profiles with energies  $E \leq E_{min}^{BCA}$ , the BCA breakdown limit calculated previously (except for F where the lowest energy available is 1keV) while Figs 3b to 8b show profiles with energies above this limit. It should be noted that at least part of the surface spike in the P profiles is SIMS artifact and merged into the actual peak, resulting in the high surface concentration. The poor agreement in the tail region of the N profiles can be attributed to the high detection limit of N. A good coherence with SIMS data is seen for almost all the MD simulated profiles, even though channeling at such low energies is pronounced. The tails of the profiles obtained from MD agree very well with the experimental data (except N), while profiles generated from the BCA code tend to underestimate the degree of channeling at low energies, deviating from the SIMS by at least half an order of magnitude. Besides the inability of BCA to account for simultaneous multiple collisions significant at low energies, part of the discrepancy can be attributed to the typically used solely repulsive universal Ziegler-Biersack-Littmark (ZBL) potential (1) in BCA codes which fails to describe attractive forces that come into play as energy lowers. The non-local electronic stopping models used in BCA codes also tend to overestimate the electronic drag force in channeling directions where the electronic density is lower.

As the initial kinetic energy of the incoming ion increases, conditions limiting the use of BCA become insignificant. This is reflected in the good agreement of the simulated profiles with SIMS at higher implant energies (Figs. 3b to 8b). It also suggests that the breakdown limits calculated for the various species in

Table I provide reasonable estimates of the breakdown points. The poor agreement of BCA for N and F at any energy could be due to the lack of calibrated parameters in the electronic stopping model. Conversely speaking, the excellent agreement obtained with MD for these 2 species can be largely attributed to the local electronic model, where the phase shifts were *specifically* calculated for each target-projectile pair.

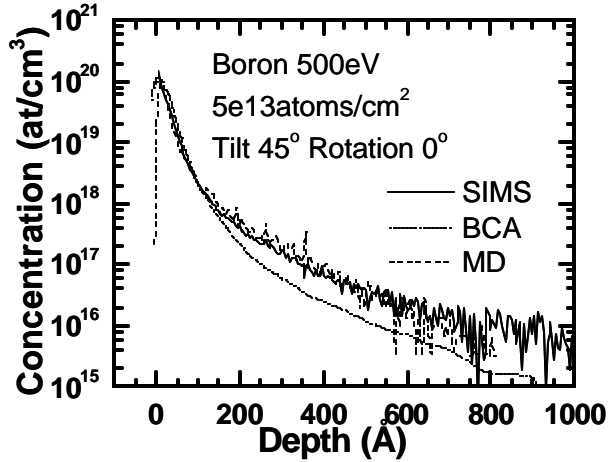


Fig. 3a Comparison with SIMS data for B 0.5keV, 5e13 atoms/cm<sup>2</sup>, 45°/0°

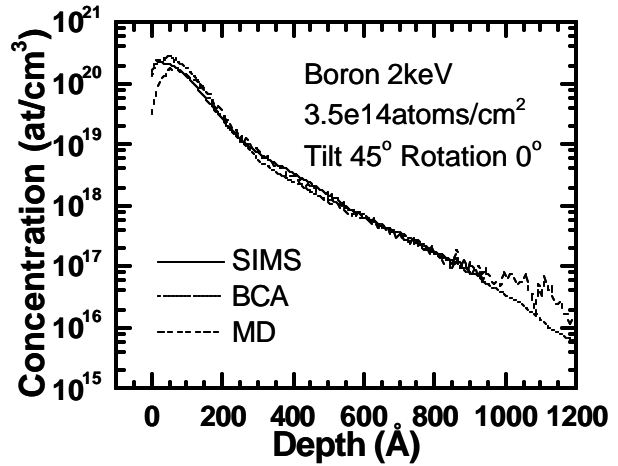


Fig. 3b Comparison with SIMS data for B 2keV, 3.5e14 atoms/cm<sup>2</sup>, 45°/0°

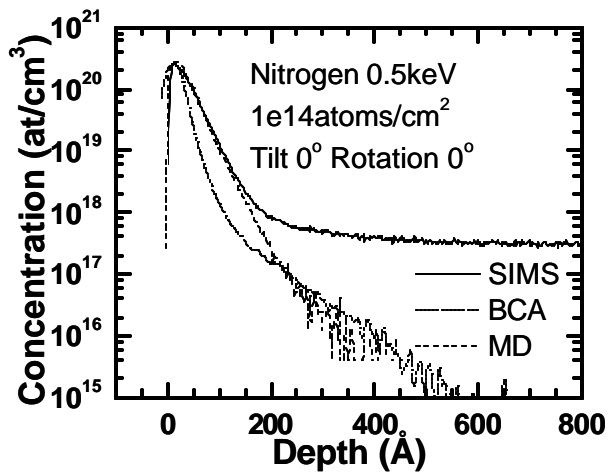


Fig. 4a Comparison with SIMS data for N 0.5keV, 1e14 atoms/cm<sup>2</sup>, 0°/0°

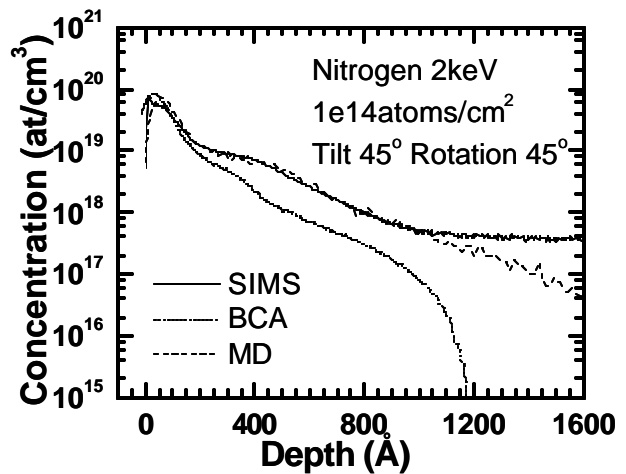


Fig. 4b Comparison with SIMS data for N 2keV, 1e14 atoms/cm<sup>2</sup>, 45°/45°

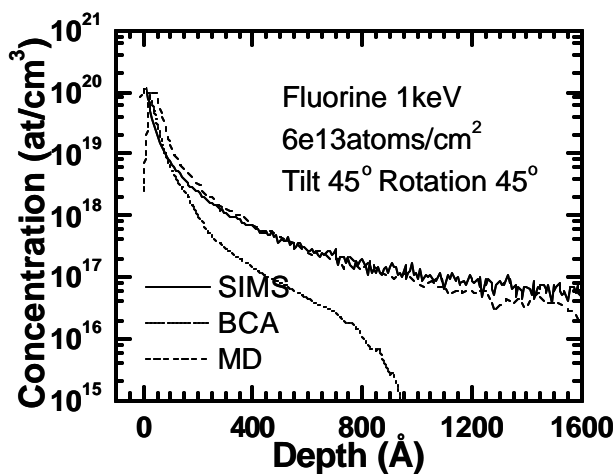


Fig. 5a Comparison with SIMS data for F 1keV, 6e13 atoms/cm<sup>2</sup>, 45°/45°

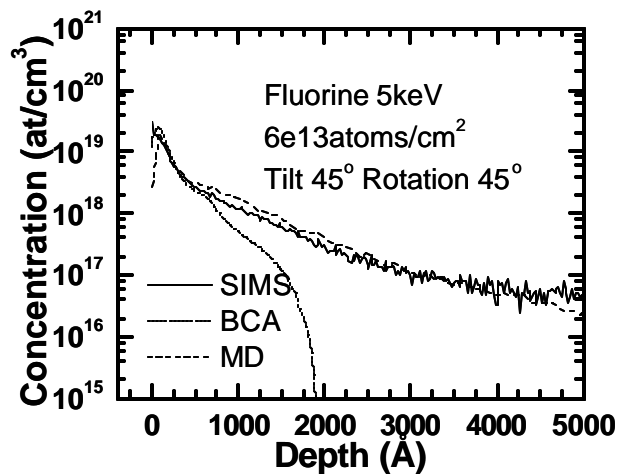


Fig. 5b Comparison with SIMS data for F 5keV, 6e13 atoms/cm<sup>2</sup>, 45°/45°

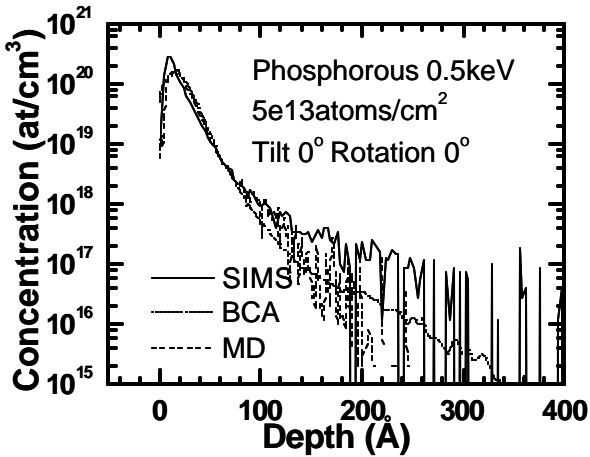


Fig. 6a Comparison with SIMS data for P 0.5keV, 5e13 atoms/cm<sup>2</sup>, 0°/0°

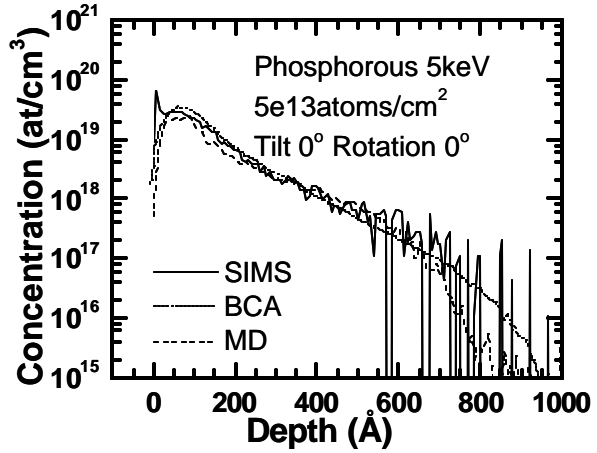


Fig. 6b Comparison with SIMS data for P 5keV, 5e13 atoms/cm<sup>2</sup>, 0°/0°

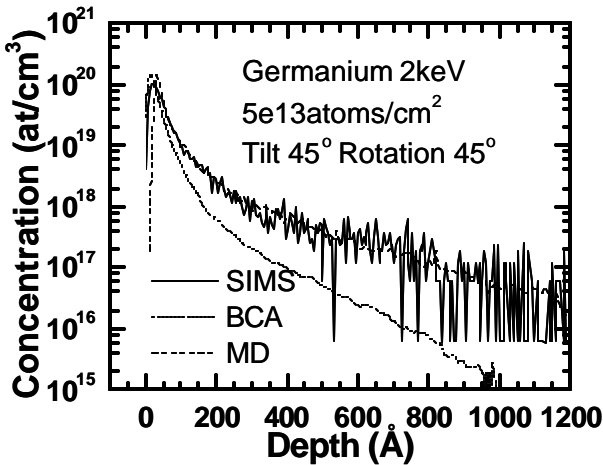


Fig. 7a Comparison with SIMS data for Ge 2keV, 5e13 atoms/cm<sup>2</sup>, 45°/45°

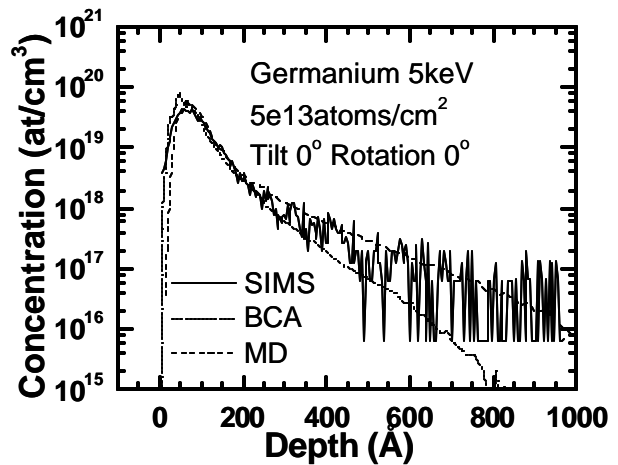


Fig. 7b Comparison with SIMS data for Ge 5keV, 5e13 atoms/cm<sup>2</sup>, 0°/0°

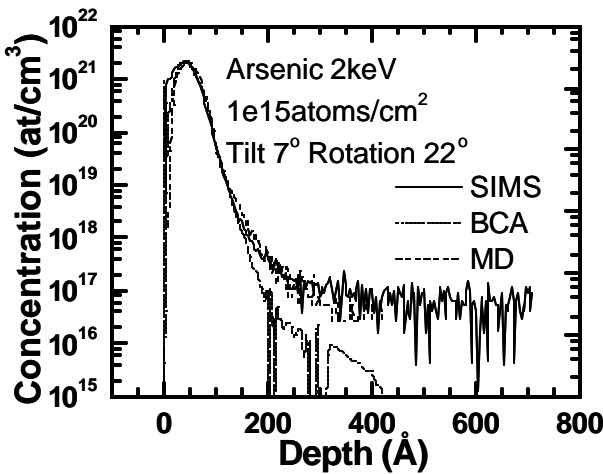


Fig. 8a Comparison with SIMS data for As 2keV, 1e15 atoms/cm<sup>2</sup>, 7°/22°

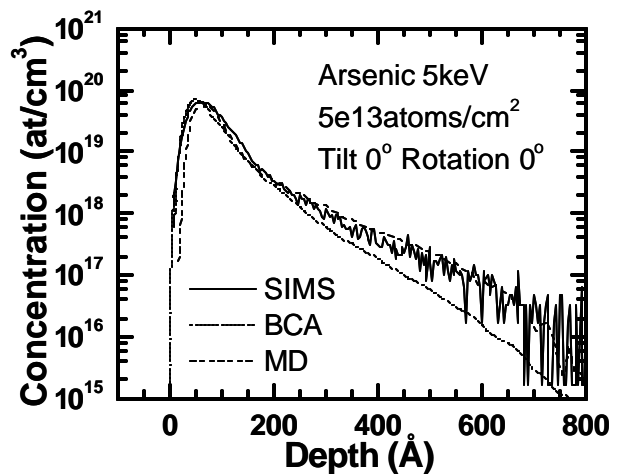


Fig. 8b Comparison with SIMS data for As 5keV, 5e13 atoms/cm<sup>2</sup>, 0°/0°

## 6. CONCLUSION

In this work, the validity of BCA at low implantation energies is questioned and further quantified by DFT calculations for various industrially important dopant species. The breakdown limits have been estimated from pair potentials regardless of crystal orientation and neighboring effects and it is shown for the first time that these DFT-calculated limits are related to the projectile's atomic weight by a power-law function. They also provide reasonable estimates as shown by comparisons with experimental data. A low energy SIMS database has been set up not only to validate this calculated limit, but also to calibrate the dopant profiles at low energies and high channeling directions. Although BCA is computationally less demanding than MD simulations, the use of the universal potential and non-local electronic models provides inaccurate descriptions of the range profiles for certain non-calibrated species and underestimates the degree of channeling in the low energy regime. On the contrary, the use of MD is not restricted to typical non-channeling implants, but its accuracy extends to describing long-ranged profiles propagated in crystal channels. MD coupled with a pair-specific local electronic stopping model makes it a robust technique to predict dopant profiles in any implant direction both at low and high energies for any species in question.

## ACKNOWLEDGMENTS

The authors would like to thank Prof. M. J. Puska and Dr J. Peltola for the electronic stopping code and all invaluable advice. All resources from Supercomputing and Visualization Unit (SVU), Institute of High Performance Computing (IHPC) and Agency of Science, Technology and Research (A\*STAR) of Singapore are gratefully acknowledged.

## REFERENCES

1. J. F. Ziegler, J. P. Biersack and U. Littmark, *The Stopping and Range of Ions in Solids*, Pergamon, New York (1985).
2. J. Lindhard, M. Scharff and H.E. Schiott, *K. Dan. Vidensk. Selsk. Mat. Fys. Medd.*, 33, 14 (1963).
3. K. Nordlund, *Comput. Mater. Sci.*, 3, 448 (1995).
4. G. Hobler and G. Betz, *Nucl. Instr. and Meth. B*, 180, 203 (2001).
5. G. Balamurugan, B.J. Obradovic, G. Wang, Y. Chen, and A.F. Tasch, *Technical Digest of IEEE 1998 IEDM*, 517 (1998).
6. B. Obradovic, G. Wang, Y. Chen, D. Li, C. Snell, and A. F. Tasch, *UT-MARLOWE Version 5.0 Manual* (1999).
7. DMOL is a trademark of Accelrys Inc. San Diego, California, USA.
8. K. Nordlund, N. Runeberg and D. Sundholm, *Nucl. Instr. and Meth. B*, 132, 45 (1997).
9. T. L. Ferrell and R. H. Richie, *Phys. Rev. B*, 16, 115 (1977).
10. M. J. Puska and R. M. Nieminen, *Phys. Rev. B*, 27, 6121 (1983).
11. J. Sillanpaa, K. Nordlund and J. Keinonen, *Phys. Rev. B*, 62, 3109 (2000).
12. K. M. Beardmore and N. Gronbech-Jensen, *Phys. Rev. E*, 57, 7278 (1998).
13. J. Sillanpaa, K. Nordlund and J. Keinonen, *Physica Scripta T79*, 272 (1999).
14. J. Peltola, K. Nordlund and J. Keinonen, *Nucl. Instr. and Meth. B*, 195, 269 (2002).
15. J. F. Ziegler, *Handbook of Ion Implantation Technology*, Elsevier Press, Amsterdam (1992).